Biomedicine & Pharmacotherapy 170 (2024) 116010

Contents lists available at ScienceDirect

Biomedicine & Pharmacotherapy

journal homepage: www.elsevier.com/locate/biopha

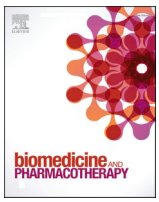

A gold-based inhibitor of oxidative phosphorylation is effective against triple negative breast cancer

R. Tyler Mertens [a], Jong Hyun Kim [a], Samuel Ofori [a,b,c,d], Chibuzor Olelewe [a,b,c,d], Paul J. Kamitsuka [b], Gunnar F. Kwakye [b], Samuel G. Awuah [a,c,d,*]

[a] Department of Chemistry, University of Kentucky; Lexington, KY 40506, United States
[b] Department of Neuroscience, Oberlin College, Oberlin, OH 44074, United States
[c] Department of Pharmaceutical Sciences, College of Pharmacy, University of Kentucky, Lexington, KY 40536, United States
[d] University of Kentucky Markey Cancer Center, USA

ARTICLE INFO

Keywords:
Gold
Mitochondria
Triple negative breast cancer
OXPHOS

ABSTRACT

Triple-negative breast cancer (TNBC) is associated with metabolic heterogeneity and poor prognosis with limited treatment options. New treatment paradigms for TNBC remains an unmet need. Thus, therapeutics that target metabolism are particularly attractive approaches. We previously designed organometallic Au(III) compounds capable of modulating mitochondrial respiration by ligand tuning with high anticancer potency in vitro and in vivo. Here, we show that an efficacious Au(III) dithiocarbamate (AuDTC) compound induce mitochondrial dysfunction and oxidative damage in cancer cells. Efficacy of AuDTC in TNBC mouse models harboring mitochondrial oxidative phosphorylation (OXPHOS) dependence and metabolic heterogeneity establishes its therapeutic potential following systemic delivery. This provides evidence that AuDTC is an effective modulator of mitochondrial respiration worthy of clinical development in the context of TNBC.

One sentence summary: Metabolic-targeting of triple-negative breast cancer by gold anticancer agent may provide efficacious therapy.

1. Introduction

Targeting cellular metabolism has become the focus of biomedicine as many cancer types depend on both glycolysis and oxidative phosphorylation (OXPHOS) to meet the high energy demand for proliferation [1–3]. Conventional thought within the field of cancer metabolism has been that tumor cells robustly rely on glycolysis to provide the necessary building blocks for macromolecule synthesis, ATP, and NADH, which are essential to meet the energetic demands of cell proliferation in aggressive cancer types. Warburg first observed this dependency on glycolysis in the 1920′s, in which he reported an abnormally high glucose uptake and reliance on glycolysis for metabolic activity in cancer cells [4–6]. The phenomenon known as aerobic glycolysis, became what we know today as the Warburg effect. Consequently, this observation led to the understanding that mitochondria are defective in tumor cells, resulting in minimal dependence on mitochondrial metabolism for growth [7,8] and that dysfunctional mitochondria are characteristic to tumors.

This notion that all tumors have innately dysfunctional mitochondria was then challenged in the 1950′s, in which Wenner and Weinhouse elegantly demonstrated that tumor cells can effectively oxidize carbohydrates and fatty acids in transplanted tumors qualitatively or perhaps quantitatively in a manner similar to normal tissue, suggesting that tumor cells were also able to utilize OXPHOS machinery [9,10]. Recent evidence has shown that triple-negative breast cancer (TNBC) models have a high dependence on both glycolytic and oxidative based pathways, suggesting that these tumors are heterogeneous [11–13]. Several studies indicate that OXPHOS may be upregulated in highly metastatic breast cancers. Examination of complex I, II, and IV activity assayed by NADH, succinate dehydrogenase, and cytochrome oxidase histochemical staining respectively, of breast cancer tissue reveals that electron transport chain (ETC) proteins are upregulated in breast cancer cells relative to adjacent stromal and normal epithelial cells [14–16]. Therefore, a promising strategy to treat the highly metastatic cell lines is through targeting mitochondrial metabolism and function [17–20]. Investigations examining the highly efficacious small molecules metformin, Gboxin, and IACS-010759 on OXPHOS inhibition revealed that these aggressive tumors rely heavily on functional mitochondrial and

* Corresponding author at: Department of Chemistry, University of Kentucky, Lexington, KY 40506, USA.
E-mail address: awuah@uky.edu (S.G. Awuah).

https://doi.org/10.1016/j.biopha.2023.116010
Received 6 September 2023; Received in revised form 28 November 2023; Accepted 13 December 2023
Available online 20 December 2023

that loss of mitochondrial respiration is an area that can be exploited for therapeutic gain [21–27].

Gold complexes are an ever growing scaffold that have found a broad use for many pathophysiologies, yet major challenges in gold-based chemical biology are limiting factors specifically: i) lack of target identification, ii) lack of detailed mechanistic insight, and iii) incomplete knowledge of localization within biologically relevant systems [28–30]. It is typically thought that gold complexes interact with mitochondria given that they can become delocalized lipophilic cations that accumulate inside the organelle [31–34]. It has been illustrated that direct coordination of "gold" to the selenolate domain of the active site of mitochondrial thioredoxin reductase occurs, further increasing the uptake of gold(I) into the mitochondria, which results in swelling and an increased inner mitochondrial membrane potential (IMMP) [35]. In comparison to platinum complexes, it is known that gold complexes in either the gold(I) or gold(III) oxidation states, which have little to no affinity for DNA binding. Taken together, there remains a lack of mechanistic investigations of gold complexes. Not all compounds are

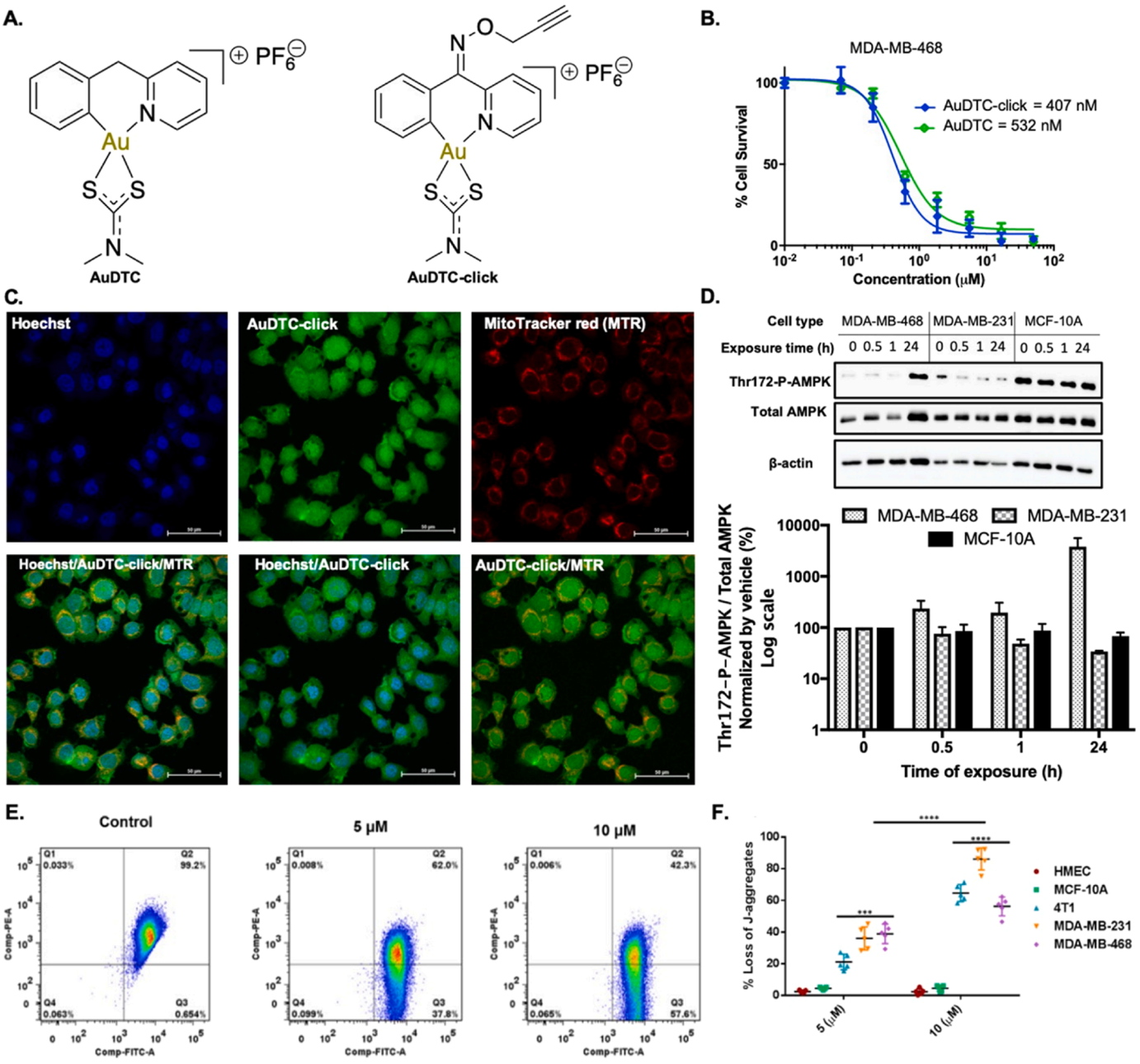

Fig. 1. AuDTC inhibits OCR and clickable AuDTC facilitates mitochondrial localization in TNBC. A) Molecular structures of AuDTC and clickable AuDTC. B) Viability of MDA-MB-468 cells after 72 h of treatment, comparing AuDTC versus AuDTC-click. Data are plotted as the mean ± s.e.m., (n = 3). IC_{50}, median inhibitory concentration. C) Click chemistry visualized with confocal microscopy in MDA-MB-468. Cells were treated for 50 μM for 1 h. Panels: i) Hoechst as the nuclear counterstain, ii) AuDTC-click – Alexa Fluor 488 azide adduct, iii) MitoTracker Red CM-H_2XRos (MTR) alone, iv) Merge of all three channels, v) Merge of Hoechst and AuDTC-click, vi) Merge of AuDTC-click and MTR. Scale bar – 50 μm. D) Western blot analyses indicate AuDTC (1 μM)-mediated activation of phospho-AMPK (pAMPK) in MDA-MB-231 cells but not MCF10A treated for the indicated time periods. $n = 3$. E) FACS analysis of MMP using JC-1 in MDA-MB-468. Loss of PE fluorescence (J-aggregates) was analyzed. F) Dot plot showing loss of PE (J-aggregates) as a percentage in comparison to the control (set as 100%). Data are plotted as the mean ± s.d., n = 5. * ** $p < 0.05$, * ** * $p < 0.01$, by an ordinary two-way ANOVA for comparison between cancer cell groups (4T1, MDA-MB-231, and MDA-MB-468) compared to normal cell groups (HMEC and MCF-10A) and an ordinary one-way ANOVA concentration for each respective cancer cell line.

created equal, therefore slight modifications and expansions of ligand systems can change the reactivity and target. We have recently reported several classes of gold complexes that selectively perturb mitochondrial respiration, mitochondrial structure, and function, as well as alter the mitochondrial electron transport chain in vivo [33,34,36,37]. Given these developments, combined with the high precedence for gold in medicine, we have focused our efforts into rigorous investigation of the biological target of these agents through in-depth biological assays.

Herein, we focused primarily on the detailed biological characterization of an organogold(III) complex bearing dithiocarbamate ligands (AuDTC) that demonstrate selective modulation of mitochondrial respiration in TNBC by targeting mitochondrial complex I. We demonstrate that metabolic reprogramming towards glycolysis is a direct consequence of the organogold(III)-induced mitochondrial dysfunction in TNBC. We provide further evidence of mitochondrial dysfunction through depolarization of membrane potential and significant ROS production, leading to the loss of key regulatory proteins and increased in oxidative DNA damage followed by mitochondrial specific cytochrome c release and apoptosis. Further, we demonstrate that AuDTC is well-tolerated in mice and inhibits TNBC xenograft tumor growth. These results indicate a potential therapeutic strategy which can be employed to alleviate adverse effects following exposure to our gold agent.

2. Results

2.1. AuDTC localizes in mitochondria of TNBC

To evaluate the cellular localization of AuDTC (Fig. 1A) and investigate its targeting modality, we developed a synthetic probe with a free alkyne as a clickable probe [38,39]. Briefly, we chemically transformed the 2-benzoylpyridine framework of the cyclometalated gold by reacting with o-2-propynylhydroxylamine hydrochloride to form an oxime bond. Replacement of the labile chloride ligands with the sodium salt of dimethyldithiocarbamate gave us an alkyne modified version of our lead compound, AuDTC, known as AuDTC-click (Fig. 1**A**). In vitro cytotoxicity of AuDTC-click in MDA-MB-468 revealed no loss in efficacy compared to the original AuDTC (Fig. 1**B**). With this new tool in hand, we sought to perform in vitro click chemistry with an azide fluorophore and counterstain with MitoTracker Red CM-H_2XRos (MTR) to see the correlation between the two dyes. We found a large amount of orange to yellow fluorescence overlap, which is indicative of colocalization between the two fluorophores with a Pearson's coefficient of 0.88 between the green and red channels (Fig. 1**C and** Figs. S1–3). Overall, this experimental design not only sets a premise for clickable gold agents that can be monitored in vitro, but also support for mitochondrial targeting by AuDTC in TNBC.

Consistent with mitochondria localization studies, AuDTC induced in human TNBC cells (MDA-MB-468) the expression of phosphorylated AMP-activated protein kinase (AMPK), a highly conserved energetic motor that is rapidly activated following mitochondrial insults, dependent or independent of mitochondrial membrane potential disruption (Fig. 1**D**). AuDTC-treated MDA-MB-468 cells showed a robust increase in AMPK and phospho-AMPK with no significant change in expression in MDA-MB-231 and MCF10A. These data indicate that AuDTC causes cellular energy defects in MDA-MB-468 but not in MDA-MB-231 or normal cells, which establishes the selectivity of AuDTC for tumor cells that depend on mitochondria metabolism for survival and the metabolic heterogeneity of TNBC.

Mitochondrial membrane potential (MMP) is critical to maintain homeostatic balance within the mitochondria. To investigate MMP, we used the fluorometric JC-1 dye that forms J-aggregates (red fluorescence) in healthy, intact mitochondria and J-monomers (green fluorescence) in cells exposed to AuDTC. Depolarization of the mitochondrial membrane potential induced by AuDTC was measured by flow cytometry in a panel of TNBCs as well as normal breast epithelial cells, MCF10A and HMEC. Specifically, following the treatment with AuDTC, we observed a large decrease in mitochondrial membrane potential (loss of PE when analyzed with flow cytometry) in MDA-MB-468 within 90 min of treatment (Fig. 1E). Upon comparison with the classic uncoupler CCCP—carbonyl cyanide *m*-chlorophenyl hydrazine—AuDTC indeed also rapidly induced a reduction in MMP by 50% at 5 μM (MDA-MB-231, MDA-MB-468 and 4T1) and 60 – 95% loss (MDA-MB-231, MDA-MB-468 and 4T1) at 10 μM within just 90 min of treatment (Fig. 1F). At high concentrations 10 μM, there was no significant loss in MMP in normal breast epithelial cells (HMEC and MCF-10A) (Fig. 1F and Figs. S4–7), illustrating high specificity towards mitochondrial dysfunction in cancer cell lines. Considering that the MMP is a key driving force regulating mitochondrial metabolism, this MMP perturbation appears to be a critical mechanism of AuDTC-induced energy deficits.

2.2. AuDTC inhibits oxidative phosphorylation in TNBC

Initial efforts to evaluate the capacity of AuDTC to potentiate the mitochondrial electron transport chain (ETC) and interact with ETC complex proteins ensued by characterizing the effect of AuDTC on cellular oxygen consumption in a broad panel of cancerous and normal cell lines. We performed oxygen consumption rate (OCR) experiments in different cell types by the addition of AuDTC in pneumatic fashion and revealed a dose-dependent depletion of OCR consistent with well-known inhibitors of OXPHOS. Despite the rapid and irreversible inhibition of OCR in TNBCs (Fig. 2**A**) and other cancer types (data not shown), AuDTC did not have an inhibitory effect on OCR in normal epithelial, fibroblast, or embryonic cells (Fig. 2**B**), indicating that AuDTC selectively and rapidly impedes OCR in cancer cells, while sparing normal cells (Fig. 2**C**).

Loss of ETC function and stability lead to the release of cytochrome c. Upon exposure of MDA-MB-468 cells to 1 μM AuDTC, we observed a 9% release of mitochondrial cytochrome c within 4 h (Fig. 2D). Time-dependent analysis and the use of bortezomib as positive control revealed a $>$ 60% increase in cytochrome c release (Fig. 2D). Western blot of AuDTC-treated MDA-MB468 cells showed downregulation of cell survival marker phospho-ERK(1/2) by 24 h (Fig. 2E) and the mitochondrial protein required for folding key proteins after import into the mitochondria, HSP60 (Fig. 2F). We posit that mitochondrial dysfunction induced by AuDTC stimulates HSP60 response and affects cell survival via downregulating phospho-ERK(1/2) [40,41]. These data suggest that AuDTC upon association with the mitochondria alters mitochondrial protein function, induces cytochrome c release, and delays activation of compensatory cell survival pathways resulting in the onset of apoptosis in TNBC cells.

2.3. AuDTC induce direct mitochondrial complex inhibition

The ability of AuDTC to inhibit mitochondrial ETC complex proteins was measured by evaluating the activity of immunocaptured ETC complexes I to V. AuDTC inhibited complex I and complex V with a Kd of 25–30 μM compared to untreated samples (Fig. 3A). We observed that AuDTC did not impact complex II, III, and IV activity. These data suggest that AuDTC specifically inhibits complex I and V, which are critical sources of ROS and ATP production, respectively.

The effect of AuDTC on mitochondrial complex I-driven respiration was evaluated using the plasma membrane permeabilizer (XF PMP) assay (Fig. 3B). To measure complex I driven OCR, we subjected MDA-MB-468 cells to pneumatic injection of AuDTC after incubation with MAS buffer containing excess levels of pyruvate (10 mM) added with 1 mM malate to feed the TCA cycle and thus NADH linked respiration. In a concentration-dependent manner, we observed a loss in OCR and respiratory function at 33 μM (Fig. 3C, purple bar) [42]. Further analyses revealed a significant loss in basal respiration and ATP production as well as loss of proton leak illustrating that complex I driven respiration is affected (Fig. 3D-F). The effect on complex I respiration is rapid at

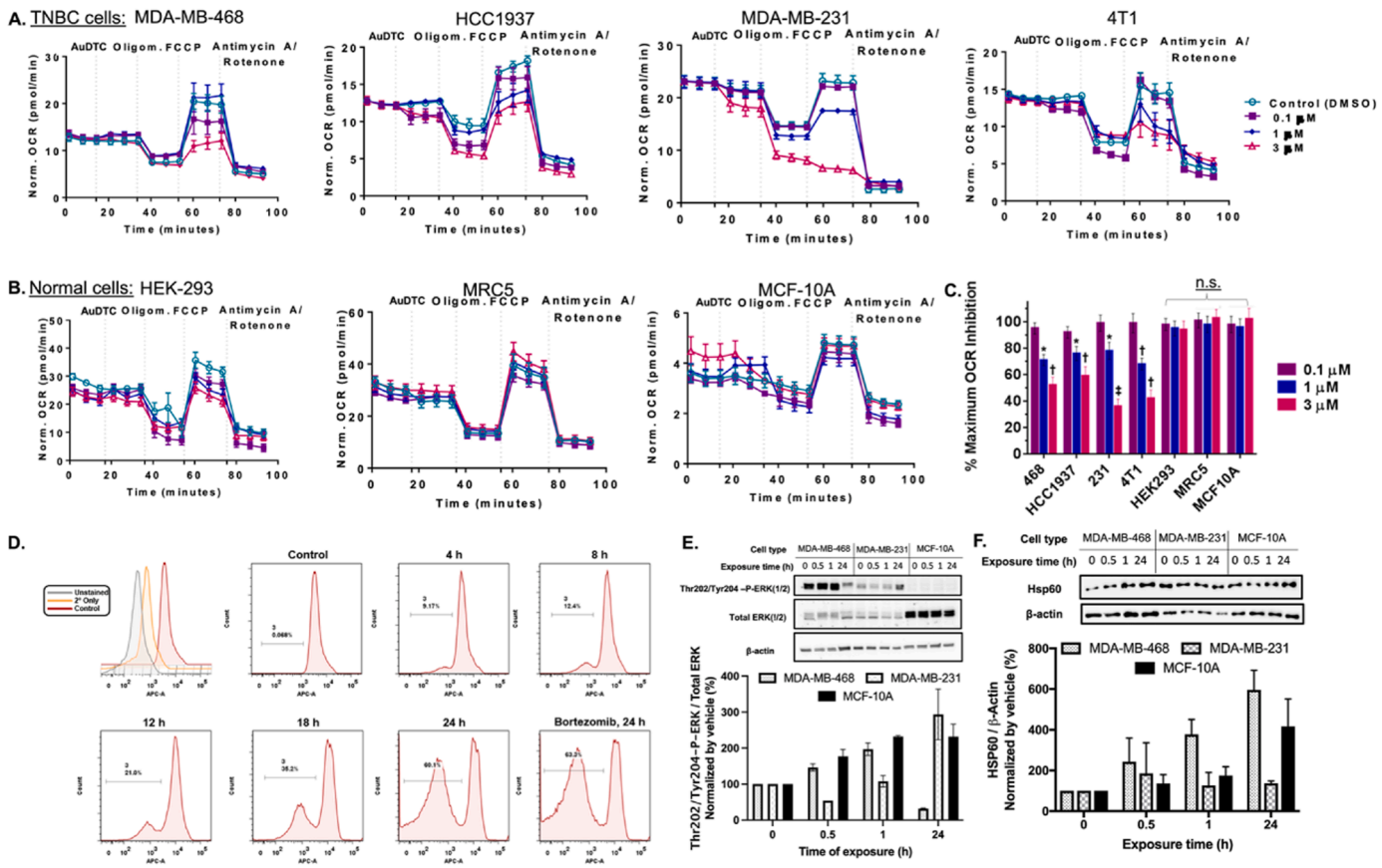

Fig. 2. AuDTC selectively inhibits cellular oxygen consumption in TNBC. A-B) Bioenergetic stress test of AuDTC in cancerous breast and normal cell lines. OCR was normalized per 1000 cells. Data are plotted as the mean ± s.e.m., n = 8. C) Maximal OCR inhibition extrapolated from the OCR data after pneumatic injection of AuDTC. Data are plotted as the mean ± s.e.m, n = 8. * $p < 0.05$, * * $p < 0.01$, * ** $p < 0.001$. n.s. = not significant, by a Student's two-tailed *t* test. D) Mitochondrial specific cytochrome c release in MDA-MB-468 after treatment with AuDTC (1 μM). E) Western blot analyses indicate AuDTC (1 μM)-mediated activation of phospho-ERK(1/2), total ERK, and F) Hsp60 in MDA-MB-468, MDA-MB-231 and MCF10A treated for the indicated time periods. $n = 3$.

33 μM with the immediate loss of ATP production (Fig. 3**F**), suggesting that this deleterious effect is not a product of long exposure and subsequent cell senescence.

2.4. AuDTC induce oxidative stress and damage in TNBC

To assess the production of reactive oxygen species (ROS), we analyzed AuDTC-induced ROS generation by using DCF-DA, a fluorogenic dye, which is cleaved by intracellular esterases and subsequently oxidized by ROS into a fluorescent molecule (Fig. 4A), and examined mitochondrial superoxide using mitosox dye (Fig. 4A). AuDTC significantly induces ROS not only in MDA-MB-468 cells but in the murine 4T1 cells (Fig. 4B) and across a variety of human breast TNBC with minimal effect on normal breast epithelial cells (Fig. 4C). Western blot of the kelch-like ECH-associated protein 1 (KEAP1), a protein that interacts with NRF2 in protecting cells from oxidative stress is upregulated in AuDTC-treated MDA-MB-468 cells (Fig. 4D).

Although ROS is required for important cell signaling events, excessive production leads to cell damage and death [43,44]. ROS can directly interact with cellular components and induce deleterious effects including DNA damage, lipid peroxidation, and protein modifications. To analyze the effects of AuDTC-induced ROS production, we assessed the impact on γH2AX activation, which results from phosphorylation of the Ser-139 residue of the histone variant H2AX, in response to DNA damage [45]. Using immunocytochemistry, we observed a persistent and significant increase in γH2AX levels and foci/nucleus at both 12 h and 24 h time points upon exposure of MDA-MB-231 cells to AuDTC (5 μM) (Fig. 4E,F). Consistent with these findings, phospho-mTOR, a key regulatory protein in maintaining cell homeostasis and proliferation and the subunit of mTORC2, and Rictor are activated in response to oxidative stress in MDA-MB-468 cells (fig. S18). Alterated autophagy leads to rapid accumulation of dysfunctional mitochondria. Thus, we examined the efficacy of AuDTC on mitochondrial autophagy (mitophagy). Our results show elevated p62 and LC3 I/II protein levels in the TNBC cells, highlighting the action of AuDTC in inducing autophagy pathways necessary to clear damaged mitochondria (Fig. 4G). Studies show that Keap1-p62-LC3 complex formation require the clearance of ubiquitin aggregates in response to oxidative stress [46]. This presents a controversy regarding the canonical role of p62, which remains to be solved [47]. We posit that AuDTC may be a useful probe to study ROS-induced p62-KEAP1-LC3 complex in cancer.

2.5. AuDTC-induced oxidative and bioenergetic stress is rescued by an antioxidant

Thus far, we demonstrated that AuDTC imposes cellular oxidative damage in TNBC with prominent mitochondrial superoxide generation. Therefore, we rationalized that the use of an antioxidant in mitoTEMPO, a mitochondrial targeting radical scavenger will mitigate deleterious effects. TNBCs were pretreated with mitoTEMPO for 2 h followed by treatment with AuDTC. Pretreatment with mitoTEMPO resulted in 1.8-fold decrease in mtROS versus the non-pretreated group (Fig. 5A). We used rotenone, a mitochondrial complex I inhibitor as positive control. Further, we analyzed the extent to which apoptosis was rescued when MDA-MB-468 cells were pre-treated with MitoTEMPO prior to AuDTC treatment. Based on previous reports combined with data suggesting

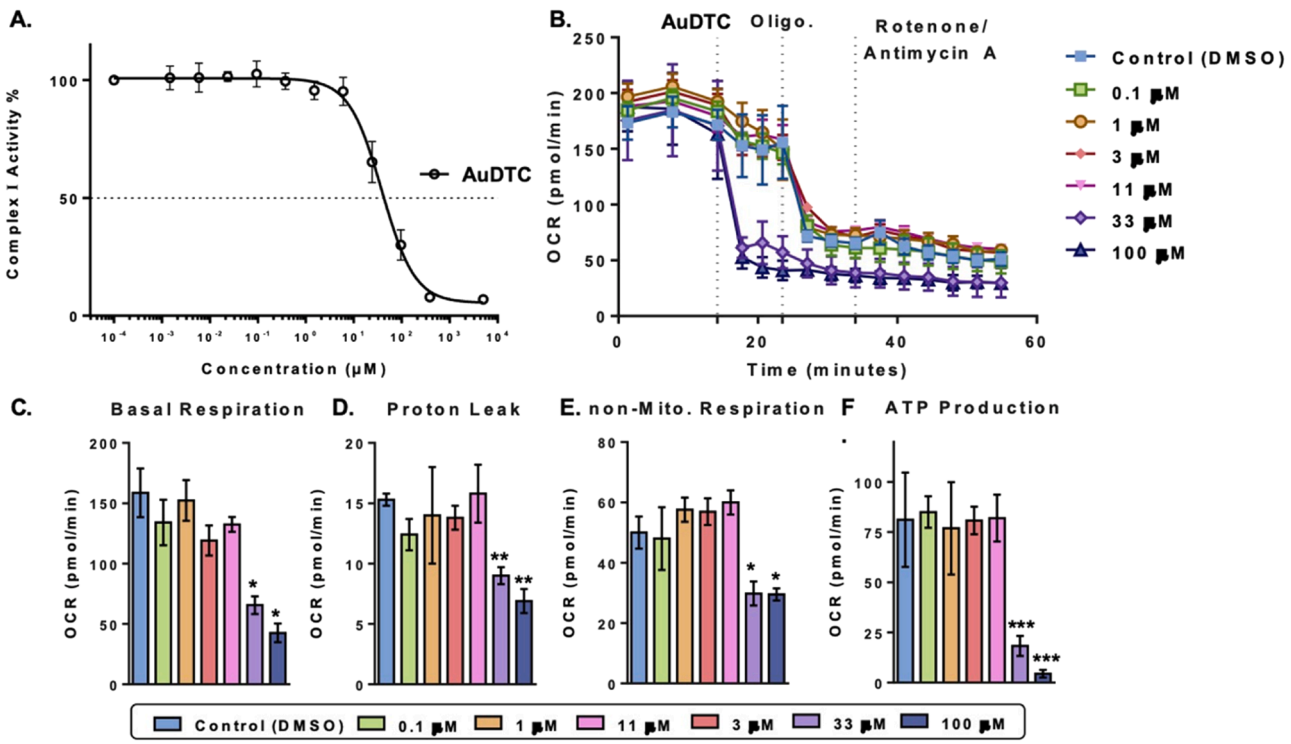

Fig. 3. AuDTC inhibits mitochondrial complex I. A) Dose-response of AuDTC on OXPHOS activity assay. B) Complex I-driven respiration measured with Seahorse XF96 in MDA-MB-468 using plasma membrane permeabilization and substrates pyruvate (10 mM)/malate (1 mM). C-F) Calculated bioenergetic parameters using OCR data from B. Data are plotted as the mean ± s.e.m., n = 8, * $p < 0.05$, * * $p < 0.01$, * ** $p < 0.001$, by an ordinary one-way ANOVA with Dunett's multiple comparis on test.

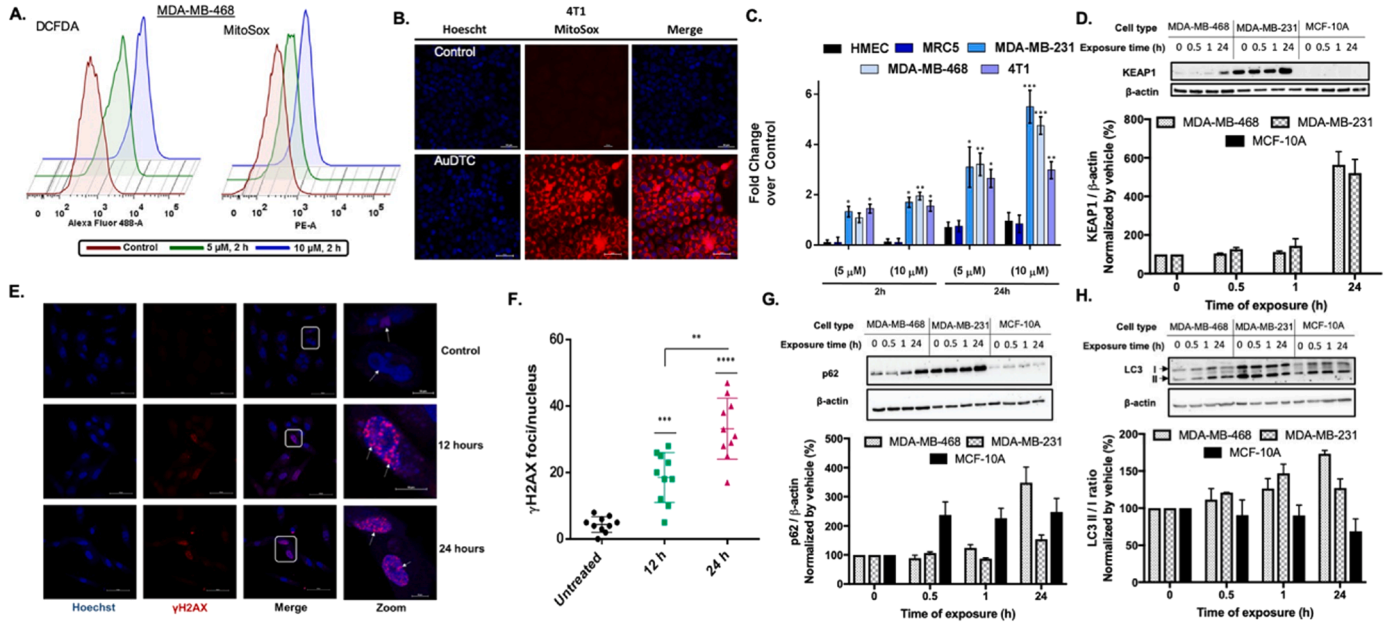

Fig. 4. AuDTC induced ROS generation and oxidative stress in TNBC. A) ROS measured by DCF-DA after 2 h treatment (FITC channel) by FACS. Gated events were kept at 30,000 for each sample. B) mtROS measured by MitoSOX after 2 h treatment (PE channel). Gated events were kept at 30,000 events. Scale bar – 10 μm. C) Bar chart of mtROS in a panel of TNBC and normal cells by FACS. D) Western blot analyses indicate AuDTC (1 μM)-mediated activation of KEAP1 in MDA-MB-468 and MDA-MB-231 cells but not MCF10A treated for the indicated time periods. $n = 3$. E) Confocal microscopy of MDA-MB-468 cells measuring increase in γH2AX foci at 12 and 24 h of treatment with AuDTC. Left to right: Hoechst stain (nuclear counterstain), γH2AX followed by fluorescent secondary antibody), merge of Hoechst and γH2AX channels, and a zoomed view of individual cells from the merged panel. All images were taken using a 60x oil objective. Scale bar – 100 μm. F) Extrapolated γH2AX foci/nucleus from E. G) Western blot analyses indicate AuDTC (1 μM)-mediated activation of p62 and H) LC3 I/II in MDA-MB-468 treated for the indicated time periods. $n = 3$.

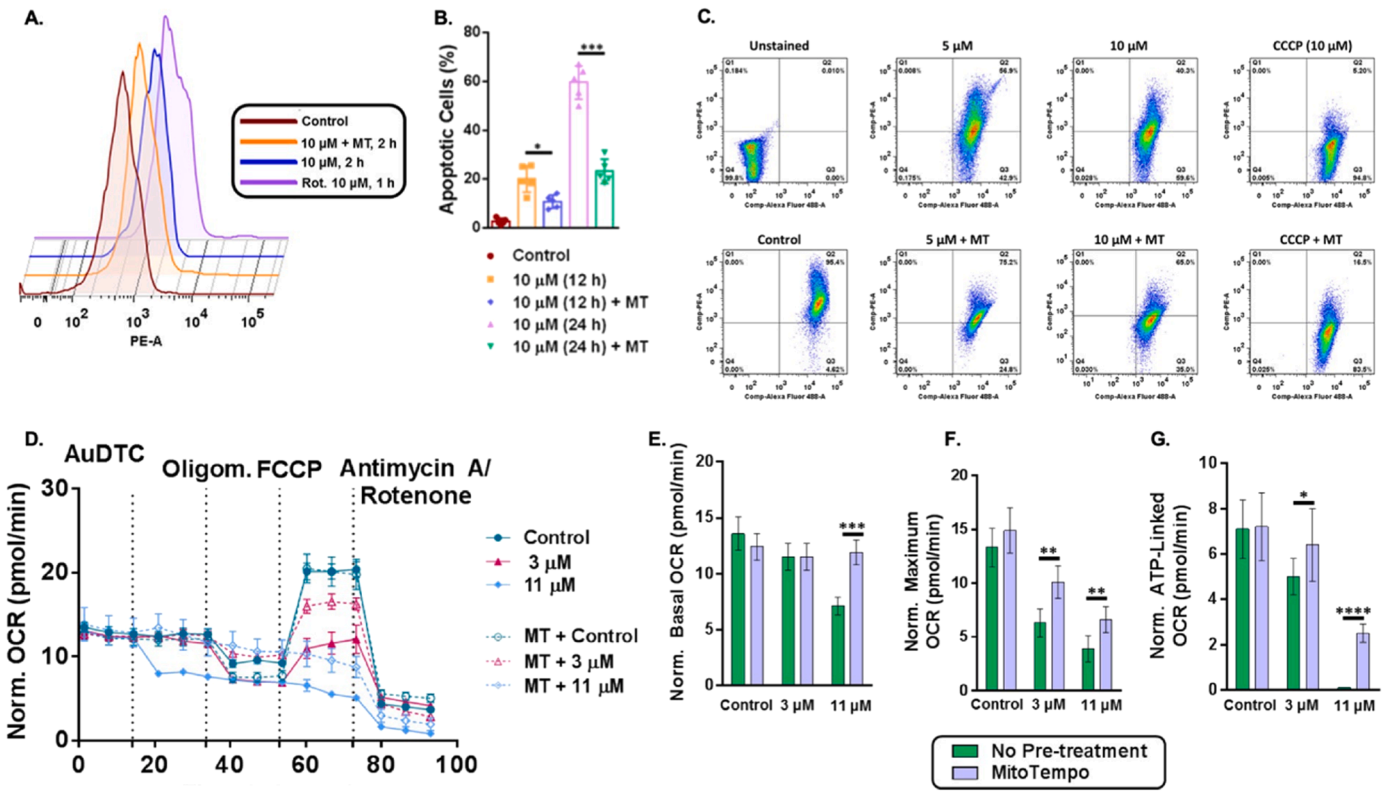

Fig. 5. MitoTempo (MT) attenuates AuDTC-induced oxidative stress and bioenergetics. A) Mitochondrial specific ROS (mtROS) measured with MitoSOX via FACS (PE channel) in MDA-MB-468. Histograms are representative of three replicates. Red bar, control; orange bar, pretreatment with MitoTEMPO for 2 h (1 μM) followed by treatment with AuDTC (10 μM, 2 h); blue bar, treatment with AuDTC (10 μM, 2 h); purple bar, a positive control rotenone (10 μM, 1 h). B) Apoptotic % calculated from FACS analysis. Data are plotted as the mean ± s.d. (n = 5), * $p < 0.05$, * ** $p < 0.001$, by an ordinary one-way ANOVA with Dunett's multiple comparison test. Gates were kept at 30,000 for each sample. C) Mitochondrial membrane depolarization monitored by loss in PE (loss in J-aggregates) using FACS in MDA-MB-468. Plots are representative of 3 replicates. D) Bioenergetic stress test using Seahorse XF96 in MDA-MB-468 with pneumatic injection of AuDTC. Solid lines represent normal experimental conditions with no pretreatment. Dashed lines represent injection of AuDTC after pretreatment with MitoTEMPO (1 μM, 2 h). OCR was normalized per 1000 cells. Data are plotted as the mean ± s.d., (n = 8). E-G) Bioenergetic parameters calculated from changes in OCR. Green bars represent the no pretreatment condition, purple bars represent the pretreatment condition. Data are plotted as the mean ± s.e.m., (n = 8), * $p < 0.05$, * * $p < 0.01$, * ** * $p < 0.0001$, by a Student's two-sided *t* test.

high mtROS production and cytochrome C release, we hypothesized that a significant portion of apoptotic cells were signaled through the mtROS signaling pathway. Pre-treatment with MitoTEMPO prior to 10 μM AuDTC treatment resulted in a significant decrease in apoptotic populations at both the 12- and 24-hour treatment conditions when exposed to 10 μM AuDTC (Fig. 5B). This confirms our hypothesis, that the mtROS is a critical inducer of cell death in the TNBC cells.

Similar experiments that measured MMP following pretreatment with MitoTEMPO (1 μM, 2 h) and AuDTC led to a 18% and 24% decrease in depolarized MMP in a dose-dependent manner. This rescue of MMP suggests that a significant portion of membrane depolarization is due to mtROS production. When CCCP was used as a control, only a small decrease from 95% to 84% was observed, suggesting that even though AuDTC and CCCP induce loss of MMP, they may do so via distinct cellular mechanisms (Fig. 5C).

Finally, we explored the possibility of the antioxidant in modulating bioenergetic stress. To do this, MDA-MB-468 cells were pretreated with MitoTEMPO (1 μM, 2 h) followed by pneumatic injection of AuDTC. MitoTEMPO was able to alleviate significant loss in OCR in comparison to the non-pretreated group (Fig. 5D). Even at an injection of 11 μM, basal OCR was rescued near to vehicle treated levels, with significant increase in OCR compared to the non-pretreated 11 μM (Fig. 5E). Furthermore, maximal OCR inhibition was significantly rescued by more than 35% in the 3 μM group and > 20% in the 11 μM MitoTEMPO group, illustrating that the functional capacity of the cell could be rescued from mtROS scavenging (Fig. 5F). ATP-linked respiration was also significantly rescued in both pretreated groups, again illustrating the ability to restore ETC function (Fig. 5G). These data represent a key dynamic of cell function upon exposure to AuDTC, in that scavenging mtROS rescues bioenergetic health and ETC function. This provides a potential future template in clinical models, given that deleterious side effects of drug treatments can be mitigated with mtROS scavengers.

2.6. AuDTC induce glycolytic shift and metabolic reprogramming

Drawing back to the dependency of cancer cells on both aerobic glycolysis and cellular metabolism, we studied the fundamental changes in cellular response upon exposure to our gold agent in the context of metabolic reprogramming. We first performed the glycolytic rate assay in MDA-MB-231, a classic TNBC cell line which has a higher dependency on glycolysis than OXPHOS for tumorigenesis (Fig. 6A). Cells were incubated with the glycolytic rate assay medium, containing substrates that are critical for glycolysis (glutamine, glucose, and pyruvate) as well as HEPES buffer. AuDTC was pneumatically injected and the change in basal rates subsequently recorded. Next, OXPHOS inhibitors were injected to inhibit mitochondrial oxygen consumption and the rate of proton efflux from respiration (PER) calculated and removed from total PER to give the glycoPER. This injection was then followed by 2-deoxy-glucose (2-DG) to block glycolytic acidification and confirm pathway specificity. The observed decrease in PER (Fig. 6A) points to a glycolytic shift. However, AuDTC injection does not alter basal rate of PER (Fig. 6B), suggesting that this compound does not directly inhibit

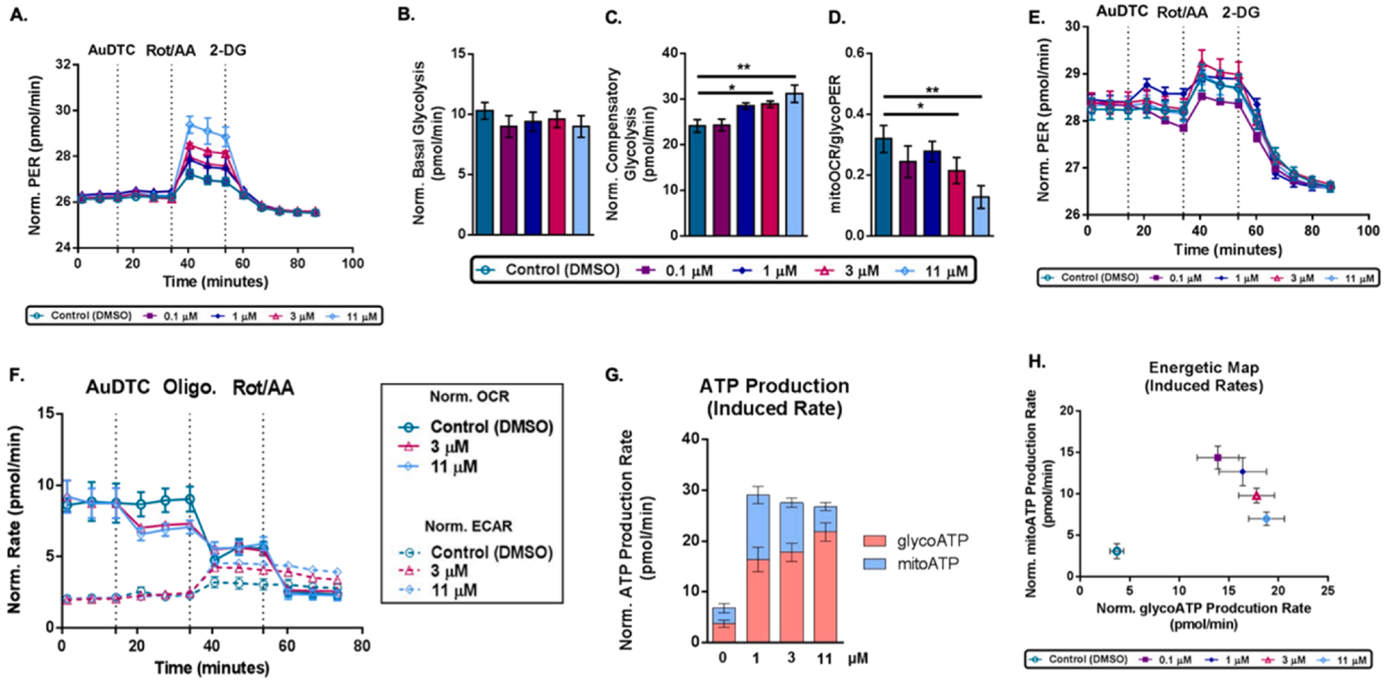

Fig. 6. Cellular energy and metabolic shift induced by AuDTC. A) Glycolytic rate of AuDTC after pneumatic injection in MDA-MB-231, a highly glycolytic cell line, in varying concentrations. PER was normalized per 1000 cells. Data are plotted as the mean ± s.e.m., n = 8. B) Basal glycolysis, time period between AuDTC and rotenone/antimycin a (Rot./AA), C) Compensatory glycolysis, time period from Rot/AA to 2-deoxyglucose (2-DG), D) mitoOCR/glycoPER ratio. Data are plotted as the mean ± s.d., n = 8. * $p < 0.05$, * * $p < 0.01$, by a Student's two-tailed *t* test in respect to the control. E) Glycolytic rate of AuDTC after pneumatic injection in HMEC, a normal human breast epithelial cell line, in varying concentrations. PER was normalized per 1000 cells. Data are plotted as the mean ± s.e.m., n = 8. F) Real time ATP rate of AuDTC after pneumatic injection in MDA-MB-468. Solid lines represent flux in OCR (mitochondrial related ATP – mitoATP). Dashed lines represent flux in ECAR (glycolytic based ATP – glycoATP). OCR and ECAR rates were normalized per 1000 cells. Data are plotted as the mean ± s.e.m., n = 8. G.) Mitochondrial and glycolytic ATP rates calculated from the real time ATP rate assay in MDA-MB-468. Red bars represent glycoATP rates and blue bars represent mitoATP rates. H) Bioenergetic map of MDA-MB-468 after treatment with AuDTC. ATP rates are normalized per 1000 cells. All rates plotted are induced rates.

glycolysis. However, compensatory glycolysis referred to as glycoPER is observed at 1.4-fold and 1.7-fold following the treatment of AuDTC at 3 μM and 11 μM respectively (Fig. 6C). Analysis of the mitoOCR/glycoPER ratio revealed a decrease with increasing concentration of AuDTC (Fig. 6D). 'Given that mitoOCR represents a measure of OXPHOS activity, the observed concentration dependent decrease in mitoOCR/glycoPER ratio in AuDTC treated cells indicates OXPHOS inhibition by AuDTC." Importantly, AuDTC does not induce a glycoPER shift in normal breast epithelial model, HMEC, in a similar glycolytic stress test (Fig. 6E). This data suggests that AuDTC does not directly affect glycolysis; however, a downstream effect is to shift the cellular metabolism to more glycolytic demand due to the loss in mitochondrial respiration.

To characterize cellular energy demands upon exposure to AuDTC, we used the Seahorse XF analyzer to investigate ATP production rates linked to both glycolysis and mitochondrial metabolism in MDA-MB-468 (Fig. 6E). AuDTC rapidly and robustly decrease basal mitoATP (represented by OCR) can be observed (Fig. 6F, solid lines) followed by no change in glycoATP (represented by ECAR) (Fig. 6F, dashed lines). Extrapolated real-time ATP rate results show > 10-fold induced rate of glycoATP coupled with loss of mitoATP, illustrating a metabolic shift towards glycolysis; a result which is indicative of an impaired ETC induced by AuDTC (Fig. 6G, H).

2.7. AuDTC inhibits growth of mouse and human TNBC

To determine the safety and therapeutic potential of AuDTC as a single agent administered in vivo, we utilized a subcutaneous xenograft mouse model of human MDA-MB-468 cells, which is a basal A molecular classification and BRCA1 wild type with P53 mutation and PTEN homo deletion. Upon establishment of the tumors (average tumor size of 50 mm^3), mice were randomized for systemic administration with AuDTC, cisplatin or vehicle control, which were administered three times a week by intraperitoneal administration. During the experiments, AuDTC treated mice showed reduced tumor growth as indicated by tumor volume measurements (Fig. 7A-C). Furthermore, the dosing schedule of AuDTC was well tolerated at the dosing schedule used as monitored through changes in body weight (Fig. 7D) and pathology examination of the heart, lung, liver, spleen, kidney (Fig. 7E). As shown in Fig. 7F, we observed significant gold accumulation in the liver, spleen, kidney, and tumor with low detection of gold in the heart or lung as measured by graphite-furnace atomic absorption spectroscopy (GFAAS). The lipophilic character of AuDTC may suggest clearance by the liver and processed through the spleen ad kidneys. The lower detection in the heart and lung is indicative of reduced cardiac and respiratory toxicity of AuDTC. The metastatic mouse-derived TNBC cell line, 4T1-iRFP were also injected into the flanks of immunocompetent mice in the presence of Matrigel. Following the appearance of visible tumors after 3 days, AuDTC was administered every other day at 10 mg/kg via intravenous injection, IV, which resulted in significant attenuation of tumor growth with no signs of visible toxicity (Fig. 7 G-I). Chemotherapy represents a major conventional treatment regimen in patients with the transition metal-based drug, cisplatin used in the treatment of metastatic TNBC. Thus, we compared the efficacy of AuDTC to the platinum agent cisplatin. Although cisplatin slowed tumor growth, signs of adverse effect as assessed by reduced body weight over the treatment period were observed. Taken together, these studies demonstrate the therapeutic promise of AuDTC for the treatment of aggressive cancer such as TNBC.

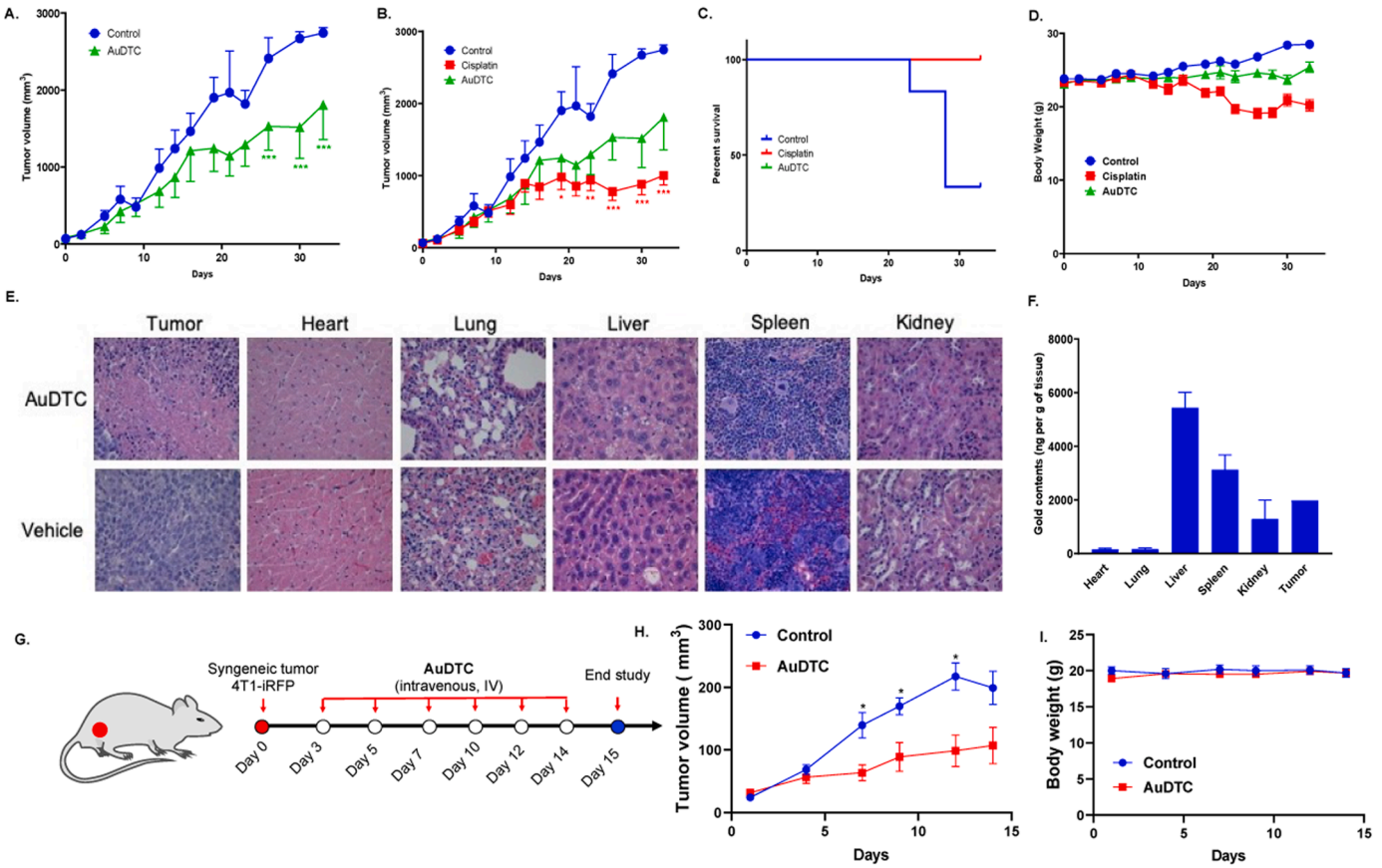

Fig. 7. Intraperitoneal treatment of AuDTC and cisplatin promote survival in a triple negative breast cancer xenograft model. (A) Relative tumor volume is reduced in mice with established MDA-MB-468 xenografts treated with AuDTC (10 mg/kg) three times per week (AuDTC, green triangles) ($n = 6$ per group). (B) Relative tumor volume of vehicle-treated (open circles), cisplatin–treated (open squares), AuDTC-treated (10 mg/kg; green triangles). Mean and 95% confidence interval are shown, and statistical significance compared to vehicle-treated group at each time point was calculated by a two-tailed unpaired Student's *t* test (A and B). (C) Kaplan-Meier survival curve, and the statistical significance was determined by a log-rank test. (D) Body weight of MDA-MB-468 xenograft bearing mice during the efficacy study. (E) H&E staining of representative tissues following AuDTC treatment. (F) Tissue biodistribution of gold at the endpoint of the study. (G) Dosing schedule of AuDTC in 4T1-iRFP tumor bearing mice. (H) Relative tumor volume is reduced in mice with established 4T1-iRFP allograft treated with AuDTC (10 mg/kg) three times per week (AuDTC, red squares) ($n = 4$ per group). (**I**) Body weight of 4T1-iRFP allograft bearing mice during the efficacy study. * $P < 0.05$, * * $P < 0.01$, * ** $P < 0.005$, and * ** * $P < 0.001$.

3. Discussion

Triple negative breast cancer (TNBC) remains an aggressive and recalcitrant form of breast cancer that lacks ER, PR, and HER2, thus rendering targeted therapy a herculean task to achieve. TNBC has prevalence in younger women, frequent reoccurrence, worst outcomes, and possess metabolic heterogeneity. Metabolic reprogramming is a hallmark of cancer and exploiting metabolic vulnerabilities in cancer is a fruitful therapeutic enterprise from the perspective of drug discovery, single therapy agent, and combination therapy in the clinic.

Breast cancer therapy is stymied by resistance largely due to reprogramming of metabolism to adapt to drug-induced insults [48]. Accumulating evidence support the role of glucose metabolism reprogramming in promoting resistance to angiogenesis therapy, doxorubicin and Phosphoinositide 3-kinase alpha (PI3Ka) inhibitors via lactate accumulation mechanisms and increased Hypoxia-inducible factor 1-alpha (HIF-1a) that characterize high glycolytic drug resistant breast cancer [49,50]. Lipid reprogramming in tumors promotes stemness and chemotherapy resistance through various mechanisms including the upregulation of fatty acid transporter CD36 [51,52]. Evidence for amino acid alteration in breast cancer and drug resistance has been established through changes in amino acid transporters such as glutamine transporter serotonin N-acetyltransferase-2 (SNAT2), basic amino acid transporter SLC6A14, and SLC1A2 transporter [53–55]. Importantly, rewiring of mitochondrial oxidative phosphorylation leads to drug resistance in breast cancer [56,57]. Inhibition of mitochondrial metabolism in combination with TB Domain and CNC Homolog 1 (BACH1) targeting is effective against TNBC [19]. Additionally, elevated activity of MYC and MCL1 in TNBC drive mitochondrial biogenesis and OXPHOS, leading to ROS production that potentiate drug response. Mitochondrial metabolism is an attractive target in cancer, thus the development of novel, clinically, relevant inhibitors is an unmet need.

Development of small molecules that target OXPHOS has gained traction with a few in clinical trials for different cancer indications. The low potency of metformin, known to also inhibit mitochondrial complex I has prompted the discovery of new chemical agents. Targeting the electron transport chain is still a challenge due to the complexity of the mitochondrial inner membrane complex proteins. Despite the increase in the discovery of OXPHOS inhibitors for cancer therapy, the in vivo response to OXPHOS inhibitors in the context of TNBC remains to be fully realized.

We previously designed unique gold-based structural scaffolds that modulate distinct pathways of the mitochondria. The organometallic gold(III) dithiocarbamates (AuDTC) framework selectively inhibited mitochondrial respiration in the MDA-MB-231 TNBC line, providing impetus to examine the translational potential of AuDTC as a new therapeutic regimen for TNBC. While gold compounds have been shown to modulate mitochondria, the specific pathways have been elusive. Our

discovery and chemical characterization of AuDTC addresses the rational design of gold-based compounds to inhibit OXPHOS. The compounds show improved stability under physiological conditions and well-tolerated in mice.

AuDTC relies on its overall positive charge and lipophilic character to accumulate in the mitochondria of TNBC with a rapid and irreversible disruption of mitochondrial respiration, leading to $>$ 30-fold selectively for TNBC models compared to normal breast epithelial cells. The manifestations of mitochondrial dysfunction due to complex I inhibition by AuDTC are mitochondrial membrane depolarization, increase in mtROS, and oxidative stress in TNBCs with loss in OXPHOS efficiency. The capability of rescuing oxidative stress with MitoTEMPO further suggests pathway specificity to mtROS induced bioenergetics stress. Altogether, these agents will be useful for future development and application to TNBC sub-types or other cancer types that rely heavily on OXPHOS for energy demands. AuDTC as result of its selective mitochondrial inhibition induce glycolytic shift as a compensatory mechanism. This unveils a mechanism of action for targeting TNBC tumors which are dependent on OXPHOS or respond to inner mitochondrial membrane disruption by combining with glycolysis inhibitors. Alterations in TNBC OXPHOS metabolism may be targeted by AuDTC in an efficacious manner.

Human tumor xenografts of TNBC are often refractory toward chemotherapy. AuDTC exhibited TNBC toxicity and tumor growth inhibition with improved survival, suggesting that an improved delivery and combination with other antitumor treatment regimen may contribute to complete tumor ablation. Importantly, the elucidated mechanism of AuDTC associated toxicity in TNBC conveys a much broader utility of this gold-based agent in different cancer subtypes beyond TNBC.

4. Materials and methods

4.1. Study design

The design of this study was to validate AuDTC as therapeutic regimen for TNBC. The efficacy of AuDTC was established using in vitro and in vivo models of TNBC. For in vitro assays, we conducted experiments at a minimum of three biological replicates. In the case of in vivo models, we used a subcutaneous xenograft mouse model of human MDA-MB-468 cells, which are basal A molecular classification, BRCA1 wildtype, P53-mutated, PTEN homo deletion and high OCR rates, demonstrating high OXPHOS dependence. An allograft metastatic model of murine 4T1-iRFP cells was also established for efficacy studies. All the animal studies were performed under strict accordance with IACUC guidelines and the 3 R rule of replacement, reduction, and refinement. Mice were housed and treated according to the protocol approved by the University of Kentucky IACUC committee, USA.

For in vivo experiments, 6 mice were used per treatment group and were randomized by tumor size and weight. Female mice were used to recapitulate the hormonal and genetic make-up of TNBC, which is predominant in women. For compliance and ethical reasons, we ended experiments when tumor volume surpassed 2000 mm^3. We did not conduct experiments in a blinded fashion.

4.2. Mice

For the experiments using the subcutaneous xenograft mouse model of TNBC, 2×10^6 MDA-MB-468 cells or allograft mouse model of metastatic TNBC, 500, 000 cells were inoculated subcutaneously to the dorsal flank of 8-week-old athymic nude mice or 6-week-old Balb/c mice (Jackson lab, USA) respectively. Once the tumors were established, mice were randomized for treatment. Intraperitoneal or intravenous administrations of vehicle and therapeutic agents were performed in a volume of 200 μl.

4.3. Therapeutic impact study

The therapeutic efficacy of AuDTC was performed by randomization according to weight and tumor burden at treatment onset. AuDTC was administered intraperitoneally or intravenously at a dose of 10 mg/kg three times per week for four consecutive weeks. Cisplatin was administered intraperitoneally twice per week at 3 mg/kg. To evaluate the therapeutic tolerance of AuDTC after systemic administration, the body weight of mice was measured every other day. After the study, tissues were harvested and fixed for histological analysis or flash frozen for graphite furnace atomic absorption spectroscopy (GF-AAS) to assess gold biodistribution.

4.4. Statistical analysis

All analyses and graphs in this study were performed using the GraphPad Prism 7 software. Differences in study sample average values were analyzed using Student's *t* test or analysis of variance (parametric). This was applied in both in vitro and in vivo studies performed. We applied the *F* test to calculate the difference in the variances of the groups in the animal study. While the use of statistical methods to predetermine sample size in animal studies was not employed, we did make efforts to achieve scientific goals using the minimum number of animals.

Funding

National Institutes of Health-NCI grant R01CA258421-01 (S.G.A.), and Oberlin College (G.F.K.). The authors also acknowledge support of the Center for Pharmaceutical Research and Innovation (CPRI, NIH P20 GM130456).

CRediT authorship contribution statement

Kim Jong H: Formal analysis, Methodology. **Mertens R. Tyler:** Conceptualization, Data curation, Formal analysis, Investigation, Methodology, Project administration, Writing – original draft, Writing – review & editing. **Olelewe Chibuzor:** Formal analysis, Methodology. **Ofori Samuel:** Formal analysis, Methodology. **Kwakye Gunnar:** Formal analysis, Methodology, Writing – review & editing. **Kamitsuka Paul J.:** Methodology. **Awuah Samuel:** Conceptualization, Data curation, Formal analysis, Funding acquisition, Investigation, Methodology, Project administration, Resources, Supervision, Validation, Visualization, Writing – original draft, Writing – review & editing.

Declaration of Competing Interest

The authors declare the following financial interests/personal relationships which may be considered as potential competing interests: The authors declare the following competing financial interest(s): S.G.A. has patents pending to University of Kentucky Research Foundation. S.G.A. serves on the advisory board and is Chief Science Officer for Phronesis AI.

Data Availability

AuDTC is available from S.G.A.'s laboratory. All reasonable requests for collaboration involving materials used in the research will be fulfilled contingent on written requests that comply with patent applications of AuDTC and the University of Kentucky. Any such inquiries or requests should be directed to the corresponding author. All data associated with this study are present in the paper or Supplementary Materials.

Acknowledgments

We thank all the core facilities at the University of Kentucky who provided support in completion of the experiments detailed in this manuscript. Specifically, the UK NMR Center supported by NSF (CHE-997738) and the UK X-ray facility supported by the MRI program from NSF (CHE-1625732), flow cytometry and immune function core supported by the Office of the Vice President of Research, the Markey Cancer Center, and NCI Center Core Support Grant (P30 CA177558), and the microscopy facilities (UK Light Microscopy Core) for their assistance. We thank Dr. Tomoko Sengoku and Mr. Michael Alstott for their support with our redox metabolism experiments, supported by the shared resource(s) of the University of Kentucky Markey Cancer Center (P30CA177558). We are grateful for the use of Dr Steven Van Lanen's laboratory (UK College of Pharmacy) LC-MS.

Author contributions

RTM and SGA designed the study. R.T.M., J-H.K., S.O., C.O., P.J.K., G.F.K., performed and contributed to the analysis of the experimental results. R.T.M. and S.G.A. wrote the manuscript with comments from all authors.

Appendix A. Supporting information

Supplementary data associated with this article can be found in the online version at doi:10.1016/j.biopha.2023.116010.

References

[1] Y. Zhao, E.B. Butler, M. Tan, Targeting cellular metabolism to improve cancer therapeutics, e532-e532, Cell Death Dis. 4 (2013). e532-e532.
[2] J.B. Spinelli, M.C. Haigis, The multifaceted contributions of mitochondria to cellular metabolism, Nat. Cell Biol. 20 (2018) 745–754.
[3] S.E. Weinberg, N.S. Chandel, Targeting mitochondria metabolism for cancer therapy, Nat. Chem. Biol. 11 (2015) 9–15.
[4] O. Warburg, F. Wind, E. Negelein, The metabolism of tumors in the body, J. Gen. Physiol. 8 (1927) 519–530.
[5] M. Potter, E. Newport, K.J. Morten, The Warburg effect: 80 years on, Biochem Soc. Trans. 44 (2016) 1499–1505.
[6] P. Danhier, et al., Cancer metabolism in space and time: beyond the Warburg effect, Biochim Biophys. Acta Bioenerg. 1858 (2017) 556–572.
[7] S. Vyas, E. Zaganjor, M.C. Haigis, Mitochondria and Cancer, Cell 166 (2016) 555–566.
[8] P.E. Porporato, N. Filigheddu, J.M.B. Pedro, G. Kroemer, L. Galluzzi, Mitochondrial metabolism and cancer, Cell Res 28 (2018) 265–280.
[9] S. Weinhouse, R.H. Millington, C.E. Wenner, Metabolism of neoplastic tissue. I. The oxidation of carbohydrate and fatty acids in transplanted tumors, Cancer Res 11 (1951) 845–850.
[10] S. Weinhouse, On respiratory impairment in cancer cells, Science 124 (1956) 267–269.
[11] Y. Gong, et al., Metabolic-pathway-based subtyping of triple-negative breast cancer reveals potential therapeutic targets, 51-64 e59, Cell Metab. 33 (2021), 51-64 e59.
[12] L. Shen, et al., Metabolic reprogramming in triple-negative breast cancer through Myc suppression of TXNIP, Proc. Natl. Acad. Sci. USA 112 (2015) 5425–5430.
[13] X. Sun, et al., Metabolic reprogramming in triple-negative breast cancer, Front Oncol. 10 (2020), 428.
[14] A.F. Santidrian, et al., Mitochondrial complex I activity and NAD+/NADH balance regulate breast cancer progression, J. Clin. Invest 123 (2013) 1068–1081.
[15] D. Zhou, L. Shao, D.R. Spitz, Reactive oxygen species in normal and tumor stem cells, Adv. Cancer Res 122 (2014) 1–67.
[16] V. Raimondi, F. Ciccarese, V. Ciminale, Oncogenic pathways and the electron transport chain: a dangeROS liaison, Br. J. Cancer 122 (2020) 168–181.
[17] R.T. Mertens, S. Parkin, S.G. Awuah, Cancer cell-selective modulation of mitochondrial respiration and metabolism by potent organogold(iii) dithiocarbamates, Chem. Sci. 11 (2020) 10465–10482.
[18] J.H. Kim, et al., Anticancer gold(iii)-bisphosphine complex alters the mitochondrial electron transport chain to induce in vivo tumor inhibition, Chem. Sci. 12 (2021) 7467–7479.
[19] J. Lee, et al., Effective breast cancer combination therapy targeting BACH1 and mitochondrial metabolism, Nature 568 (2019) 254–258.
[20] R. Camarda, et al., Inhibition of fatty acid oxidation as a therapy for MYC-overexpressing triple-negative breast cancer, Nat. Med. 22 (2016) 427–432.
[21] G. Libby, et al., New users of metformin are at low risk of incident cancer: a cohort study among people with type 2 diabetes, Diabetes Care 32 (2009) 1620–1625.
[22] S. Soberanes, et al., Metformin Targets Mitochondrial Electron Transport to Reduce Air-Pollution-Induced Thrombosis, 335-347.e335, Cell Metab. 29 (2019), 335-347.e335.
[23] W.W. Wheaton, et al., Metformin inhibits mitochondrial complex I of cancer cells to reduce tumorigenesis, Elife 3 (2014), e02242.
[24] J.R. Molina, et al., An inhibitor of oxidative phosphorylation exploits cancer vulnerability, Nat. Med. 24 (2018) 1036–1046.
[25] X. Liu, I.L. Romero, L.M. Litchfield, E. Lengyel, J.W. Locasale, Metformin targets central carbon metabolism and reveals mitochondrial requirements in human cancers, Cell Metab. 24 (2016) 728–739.
[26] S.R. Lord, et al., Integrated pharmacodynamic analysis identifies two metabolic adaption pathways to metformin in breast cancer, 679-688.e674, Cell Metab. 28 (2018), 679-688.e674.
[27] Y. Shi, et al., Gboxin is an oxidative phosphorylation inhibitor that targets glioblastoma, Nature 567 (2019) 341–346.
[28] T. Zou, C.T. Lum, C.-N. Lok, J.-J. Zhang, C.-M. Che, Chemical biology of anticancer gold(iii) and gold(i) complexes, Chem. Soc. Rev. 44 (2015) 8786–8801.
[29] S. Jürgens, et al., Exploring the C^N^C theme: Synthesis and biological properties of tridentate cyclometalated gold(III) complexes, Bioorg. Med Chem. 25 (2017) 5452–5460.
[30] K.-C. Tong, et al., An anticancer gold(III)-activated porphyrin scaffold that covalently modifies protein cysteine thiols, Proc. Natl. Acad. Sci. 117 (2020) 1321–1329.
[31] J. Hyun Kim, S. Ofori, R.T. Mertens, S. Parkin, S.G. Awuah, Water-Soluble Gold (III)–metformin complex alters mitochondrial bioenergetics in breast cancer cells, ChemMedChem 16 (2021) 3222–3230.
[32] M.V. Babak, et al., Interfering with metabolic profile of triple-negative breast cancers using rationally designed metformin prodrugs, Angew. Chem. Int. Ed. 60 (2021) 13405–13413.
[33] J.H. Kim, et al., Anticancer gold(iii)-bisphosphine complex alters the mitochondrial electron transport chain to induce in vivo tumor inhibition, Chem. Sci. 12 (2021) 7467–7479.
[34] R.T. Mertens, S. Parkin, S.G. Awuah, Cancer cell-selective modulation of mitochondrial respiration and metabolism by potent organogold(iii) dithiocarbamates, Chem. Sci. 11 (2020) 10465–10482.
[35] J.L. Hickey, et al., Mitochondria-targeted chemotherapeutics: the rational design of Gold(I) N-heterocyclic carbene complexes that are selectively toxic to cancer cells and target protein selenols in preference to thiols, J. Am. Chem. Soc. 130 (2008) 12570–12571.
[36] S. Gukathasan, S. Parkin, S.G. Awuah, Cyclometalated Gold(III) Complexes Bearing DACH Ligands, Inorg. Chem. 58 (2019) 9326–9340.
[37] R.T. Mertens, et al., Synthetic control of mitochondrial dynamics: developing three-coordinate Au(I) probes for perturbation of mitochondria structure and function, JACS Au 1 (2021) 439–449.
[38] H.C. Kolb, M.G. Finn, K.B. Sharpless, Click chemistry: diverse chemical function from a few good reactions, Angew. Chem. Int. Ed. 40 (2001) 2004–2021.
[39] D.S. Tyler, et al., Click chemistry enables preclinical evaluation of targeted epigenetic therapies, Science 356 (2017) 1397–1401.
[40] C. Zhou, et al., Oncogenic HSP60 regulates mitochondrial oxidative phosphorylation to support Erk1/2 activation during pancreatic cancer cell growth, Cell Death Dis. 9 (2018), 161.
[41] Y. Tang, Y. Zhou, S. Fan, Q. Wen, The multiple roles and therapeutic potential of HSP60 in cancer, Biochem. Pharmacol. 201 (2022), 115096.
[42] N.M. Anderson, P. Mucka, J.G. Kern, H. Feng, The emerging role and targetability of the TCA cycle in cancer metabolism, Protein Cell 9 (2018) 216–237.
[43] V.J. Thannickal, B.L. Fanburg, Reactive oxygen species in cell signaling, Am. J. Physiol. Lung Cell Mol. Physiol. 279 (2000) L1005–L1028.
[44] D.G. Deavall, E.A. Martin, J.M. Horner, R. Roberts, Drug-induced oxidative stress and toxicity, J. Toxicol. 2012 (2012), 645460.
[45] C. Lu, et al., Cell apoptosis: requirement of H2AX in DNA ladder formation, but not for the activation of caspase-3, Mol. Cell 23 (2006) 121–132.
[46] W. Fan, et al., Keap1 facilitates p62-mediated ubiquitin aggregate clearance via autophagy, Autophagy 6 (2010) 614–621.
[47] T. Jiang, et al., p62 links autophagy and Nrf2 signaling, Free Radic. Biol. Med 88 (2015) 199–204.
[48] Y. Liu, Q. Zhou, S. Song, S. Tang, Integrating metabolic reprogramming and metabolic imaging to predict breast cancer therapeutic responses, Trends Endocrinol. Metab. 32 (2021) 762–775.
[49] L. Pisarsky, et al., Targeting metabolic symbiosis to overcome resistance to anti-angiogenic therapy, Cell Rep. 15 (2016) 1161–1174.
[50] M. Xu, et al., FGFR4 links glucose metabolism and chemotherapy resistance in breast cancer, Cell Physiol. Biochem 47 (2018) 151–160.
[51] W.W. Feng, et al., CD36-mediated metabolic rewiring of breast cancer cells promotes resistance to HER2-targeted therapies, 3405-3420.e3405, Cell Rep. 29 (2019), 3405-3420.e3405.
[52] T. Wang, et al., JAK/STAT3-regulated fatty acid β-oxidation is critical for breast cancer stem cell self-renewal and chemoresistance, 136-150.e135, Cell Metab. 27 (2018), 136-150.e135.
[53] M. Morotti, et al., Hypoxia-induced switch in SNAT2/SLC38A2 regulation generates endocrine resistance in breast cancer, Proc. Natl. Acad. Sci. USA 116 (2019) 12452–12461.
[54] M. Bacci, et al., Reprogramming of amino acid transporters to support aspartate and glutamate dependency sustains endocrine resistance in breast cancer, 104-118.e108, Cell Rep. 28 (2019), 104-118.e108.

[55] V. Thewes, et al., The branched-chain amino acid transaminase 1 sustains growth of antiestrogen-resistant and ERα-negative breast cancer, Oncogene 36 (2017) 4124–4134.
[56] G. Deblois, et al., ERRα mediates metabolic adaptations driving lapatinib resistance in breast cancer, Nat. Commun. 7 (2016), 12156.
[57] K.M. Lee, et al., MYC and MCL1 cooperatively promote chemotherapy-resistant breast cancer stem cells via regulation of mitochondrial oxidative phosphorylation, 633-647.e637, Cell Metab. 26 (2017), 633-647.e637.